


Influence of Stereochemistry on the Bioactivation and Glucuronidation of 4-Ipomeanol^{SI}

 Aaron M. Teitelbaum, Matthew G. McDonald, John P. Kowalski, Oliver T. Parkinson, Michele Scian, Dale Whittington, Katharina Roellecke, Helmut Hanenberg, Constanze Wiek, and Allan E. Rettie

Department of Medicinal Chemistry, School of Pharmacy, University of Washington, Seattle, Washington (A.M.T., M.G.M., J.P.K., O.T.P., M.S., D.W., A.E.R.); Department of Otorhinolaryngology and Head/Neck Surgery, Heinrich-Heine University, Düsseldorf, Germany (K.R., H.H., C.W.); and Department of Pediatrics III, University, Children's Hospital Essen, University of Duisburg-Essen, Essen, Germany (H.H.)

Received April 9, 2018; accepted November 5, 2018

ABSTRACT

A potential CYP4B1 suicide gene application in engineered T-cell treatment of blood cancers has revived interest in the use of 4-ipomeanol (IPO) in gene-directed enzyme prodrug therapy, in which disposition of the administered compound may be critical. IPO contains one chiral center at the carbon bearing a secondary alcohol group; it was of interest to determine the effect of stereochemistry on 1) CYP4B1-mediated bioactivation and 2) (UGT)-mediated glucuronidation. First, (*R*)-IPO and (*S*)-IPO were synthesized and used to assess cytotoxicity in HepG2 cells expressing rabbit CYP4B1 and re-engineered human CYP4B1, where the enantiomers were found to be equipotent. Next, a sensitive UPLC-MS/MS assay was developed to measure the IPO-glucuronide diastereomers and product stereoselectivity in human tissue microsomes. Human liver and kidney microsomes generated (*R*)- and (*S*)-IPO-glucuronide diastereomers in ratios of 57:43 and 79:21, respectively. In a panel of 13 recombinantly expressed UGTs,

UGT1A9 and UGT2B7 were the major isoforms responsible for IPO glucuronidation. (*R*)-IPO-glucuronide diastereoselectivity was apparent with each recombinant UGT, except UGT2B15 and UGT2B17, which favored the formation of (*S*)-IPO-glucuronide. Incubations with IPO and the UGT1A9-specific chemical inhibitor niflumic acid significantly decreased glucuronidation in human kidney, but only marginally in human liver microsomes, consistent with known tissue expression patterns of UGTs. We conclude that IPO glucuronidation in human kidney is mediated by UGT1A9 and UGT2B7. In human liver, it is mediated primarily by UGT2B7 and, to a lesser extent, UGT1A9 and UGT2B15. Overall, the lack of pronounced stereoselectivity for IPO's bioactivation in CYP4B1-transfected HepG2 cells, or for hepatic glucuronidation, suggests the racemate is an appropriate choice for use in suicide gene therapies.

Introduction

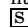
4-Ipomeanol (IPO) is a pulmonary protoxin that is produced biogenically in sweet potatoes infected with the common mold *Fusarium solani*. Consumption of moldy sweet potatoes by livestock results in selective pulmonary toxicity (mainly interstitial pneumonia and edema), which is attributed to IPO metabolic bioactivation by extrahepatic cytochrome P450 (Wilson and Burka, 1979; Devereux et al., 1982; Verschöyle et al., 1993). IPO is initially oxidized on the furan ring and

subsequently undergoes a sigmatropic ring rearrangement to form an electrophilic enedial that covalently binds to nucleophilic macromolecules in the lung (Baer et al., 2005). Other species, including rabbits, rats, guinea pigs, hamsters, and dogs, also exhibit pulmonary toxicity after IPO administration (Dutcher and Boyd, 1979; Smith et al., 1987; Gram, 1997).

Due to the selective lung toxicity observed in animal species, metabolic activation of IPO was investigated over 30 years ago in both human non-small-cell carcinoma (NCI-H322 and NCI-H358) and small-cell carcinoma cell lines (NCI-H128 and NCI-H69) (Falzon et al., 1986). Bioactivation only occurred in the non-small-cell carcinoma cultures, which prompted studies in an orthotopic xenograft mouse model of non-small-cell lung cancer (McLemore et al., 1988). In addition to providing evidence that IPO was able to inhibit the growth of tumors in the xenograft model, biopsied primary human lung carcinomas were shown to bioactivate IPO. However, during phase

This study was supported in part by the National Institutes of Health [Grant R01GM49054] and by the University of Washington School of Pharmacy Brady Fund for Natural Products. This work was also funded by the Strategische Forschungsverbund of the Heinrich Heine University (to C.W.). The authors declare no competing financial interest.

<https://doi.org/10.1124/jpet.118.249771>

 This article has supplemental material available at jpet.aspetjournals.org.

ABBREVIATIONS: CHAPS, 3-[(3-cholamidopropyl)dimethylammonio]-1-propanesulfonic acid; DLPC, 1,2-didodecanoyl-sn-glycero-3-phosphocholine; ESI, electrospray ionization; GDEPT, gene-directed enzyme prodrug therapy; HKM, human kidney microsome; HLM, human liver microsome; HPLC, high-performance liquid chromatography; HRMS, high-resolution mass spectrometry; IPO, 4-ipomeanol; KPi, potassium phosphate buffer; MRM, multiple reaction monitoring; 4-MUG, 4-methylumbelliferone glucuronide; NAC, *N*-acetyl-L-cysteine; NAL, *N*_α-acetyl-L-lysine; P450, cytochrome P450; rUGT, recombinant UGT; UDPGA, uridine 5'-diphosphoglucuronic acid; UGT, uridine 5'-diphosphoglucuronosyl transferase; UPLC-MS/MS, ultra-performance liquid chromatography-tandem mass spectrometry.

1 clinical trials involving patients with non-small-cell lung cancer (Rowinsky et al., 1993; Kasturi et al., 1998), no significant reduction in pulmonary tumors was observed, and reversible hepatotoxicity was dose limiting. In retrospect, it seems likely that IPO was ineffective in this clinical situation because humans express an unstable pulmonary cytochrome P450 4B1 enzyme (CYP4B1), which is responsible for the initial oxidation of IPO on its furan ring (Wiek et al., 2015).

In the late 1990s, interest in IPO as a potential anticancer therapeutic resurfaced because of developments in pharmacological gene therapy. This approach to cancer treatment is based on the transfection of genes for bioactivating enzymes into tumor cells, rendering them selectively susceptible to prodrugs that would otherwise be ineffective. Studies performed by Rainov et al. (1998b) provided the first evidence that transfection of rabbit *CYP4B1* into human and rat glioma cells caused them to be highly sensitive to IPO treatment. Several other groups have also shown IPO effectiveness following rabbit *CYP4B1* transfection in vitro (Smith et al., 1995; Mohr et al., 2000; Steffens et al., 2000; Frank et al., 2002; Hsu et al., 2003; Jang et al., 2010; Moon et al., 2013). Additionally, tumors from CYP4B1-expressing glioma cells implanted into nude mice exhibited abrogated growth following intraperitoneal injection of IPO (200 $\mu\text{g}/\text{day}$ for 7 days) (Rainov et al., 1998a). The most recent work on IPO in gene-directed enzyme prodrug therapy (GDEPT) concerned re-engineering of the “native” human CYP4B1 protein for maximal IPO bioactivation activity (Wiek et al., 2015; Roellecke et al., 2016). In brief, the catalytically optimized human CYP4B1 enzyme was engineered by substituting a proline residue for the native serine residue in the meandering region at position 427. Additionally, the engineered human CYP4B1 has 12 single amino acid substitutions which are coincident with human CYP4 enzymes and ultimately aid in protein stability. When introduced into human liver cells and primary T-cells, the catalytically optimized human CYP4B1 was as active as the native rabbit CYP4B1 enzyme for inducing IPO-dependent cell death.

IPO is a chiral molecule, and with the aforementioned new developments in GDEPT, it is important to understand how stereochemistry impacts IPO bioactivation and metabolism. IPO has been shown to undergo extensive glucuronidation in the rat (Statham et al., 1982), and previous work from our laboratory describes IPO glucuronidation in human liver as a potential mechanism of clearance, albeit to a much lesser extent than in a variety of other animal species (Parkinson et al., 2016). Therefore, we report the influence of stereochemistry on IPO-dependent cytotoxicity in *CYP4B1*-transduced HepG2 cells and on glucuronidation by recombinant uridine 5'-diphosphoglucuronosyl transferase (UGT) enzymes and human tissue microsomes.

Materials and Methods

Chemicals

IPO [97% purity by ^1H NMR and high-performance liquid chromatography (HPLC)–UV analysis] was a gift from the National Cancer Institute (Bethesda, MD). β -Glucuronidase from *Helix pomatia*, 4-methylumbelliferone glucuronide (4-MUG), alamethicin, ethyl- β -oxo-3-furan-propionate, (*R*)-(+)-propylene oxide, (*S*)-(+)-propylene oxide, uridine 5'-diphosphoglucuronic acid (UDPGA), 21 wt% sodium ethoxide in EtOH, *N* $_{\alpha}$ -acetyl-L-lysine (NAL), *N*-acetyl-L-cysteine (NAC), catalase,

superoxide dismutase, atazanavir, and niflumic acid were purchased from Sigma-Aldrich (St. Louis, MO). Hecogenin and fluconazole were purchased from Santa Cruz Biotechnology, Inc. (Dallas, TX). 1,2-Didodecanoyl-sn-glycero-3-phosphocholine (DLPC) was purchased from Avanti Polar Lipids (Alabaster, AL). Furfurylline was a gift from Dr. Kent Kunze (University of Washington, Seattle, WA). Dulbecco's modified Eagle's medium, fetal bovine serum, penicillin-streptomycin, and HEPES were purchased from Thermo Fisher Scientific (Waltham, MA). All solvents used for chemical reactions were reagent grade, and liquid chromatography solvents were HPLC grade.

NMR Spectroscopy and High-Resolution Mass Spectrometry

^1H and ^{13}C NMR spectra were obtained on an Agilent DD2 500 MHz NMR spectrometer (Agilent Technologies, Santa Clara, CA) at 25°C. Proton chemical shifts (δ) are reported in ppm and reference the residual proton signals of acetonitrile- d_3 ($\delta_{\text{H}} = 1.94$ ppm) or chloroform- d_3 ($\delta_{\text{H}} = 7.27$ ppm). Carbon chemical shifts reference the acetonitrile- d_3 methyl carbon signal ($\delta_{\text{C}} = 1.32$ ppm) or the chloroform- d_3 signal ($\delta_{\text{C}} = 77.16$ ppm). Coupling constants (J) are reported in Hz, and proton chemical data and multiplicities are reported as follows: s = singlet, d = doublet, t = triplet, q = quartet, and m = multiplet. High-resolution mass spectrometry (HRMS) was acquired on a Thermo Fisher LTQ Orbitrap equipped with an electrospray ionization (ESI) probe (Thermo Fisher Scientific).

Chemical Synthesis of (*R*)- and (*S*)-4-Ipomeanol

The synthetic procedure for the preparation of individual IPO enantiomers was based on the previous work described for the synthesis of racemic IPO (Alvarez-Diez and Zheng, 2004) (Supplemental Fig. 1). In brief, ethyl- β -oxo-3-furan-propionate (100 mg, 0.55 mmol) was dissolved in anhydrous EtOH (5 mL), followed by the addition of sodium ethoxide (41 mg, 0.6 mmol) and either (*R*)-(+)-propylene oxide or (*S*)-(+)-propylene oxide (670 mg, 11.5 mmol). The mixtures were stirred for 24 hours and subsequently quenched by adjusting the pH to 7 with dilute HCl. Extraction with diethylether followed by flash chromatography yielded (*R*)- and (*S*)-furyl- γ -lactone in 67% and 71% yields, respectively. In the second step, each respective lactone was hydrolyzed in the presence of 20 M sulfuric acid at 65°C for 24 hours to yield (*R*)- and (*S*)-IPO in 43% and 33% yields, respectively. Separate fractions of the (*R*)- and (*S*)-IPO were further purified by HPLC, utilizing Shimadzu LC-10ADVP pumps coupled to a Shimadzu SPD-M10AVP photodiode array detector set to 254 nm (Shimadzu, Columbia, MD). Chromatographic separation was performed with a Keystone chiral β -OH column (150 \times 2.0 mm, 5 μm ; Thermo Hypersil, Bellefonte, PA) and a 1.5-mL/min isocratic elution composed of 15% acetonitrile/85% water for a total run time of 15 minutes. (*S*)- and (*R*)-IPO were eluted at 8.0 and 7.4 minutes, respectively, under these conditions. Collected fractions were extracted with chloroform, and the structures of the recovered enantiomers were confirmed by ^1H NMR, ^{13}C NMR, and high-resolution mass spectrometry, all of which matched previously reported spectra (Boyd et al., 1972).

Effects of IPO Stereochemistry on Cytotoxicity

The cytotoxicity of (*S*)-, (*R*)-, and racemic IPO was assessed using a cell proliferation assay. HepG2 cells were modified by lentiviral transduction to express rabbit CYP4B1, re-engineered human CYP4B1 (“P+12”), or a control vector as previously described (Schmidt et al., 2015; Wiek et al., 2015; Roellecke et al., 2016). Stably transduced cells were grown in tissue culture media (Dulbecco's modified Eagle's medium, 10% fetal bovine serum, 1% penicillin-streptomycin, and 10 mM HEPES) and selected with puromycin treatment (2 $\mu\text{g}/\text{mL}$) over a 7-day period. Cells were then plated into 96 wells at 10,000 cells/well and grown for 24 hours, and the CYP4B1 line was dosed with (*S*)-, (*R*)-, and racemic IPO at final concentrations

of 100, 50, 10, 5, 1, 0.5, 0.1, 0.05, and 0.01 μM (dimethylsulfoxide did not exceed 0.1%). The control line was dosed with racemic IPO at the same concentrations. Cells were incubated for 48 hours, and the viability was determined with the CellTiter-Glo Luminescent Assay (Promega, Madison, WI). Vehicle-treated wells were set to 100% viability and LD_{50} values were calculated from dose-response curves using nonlinear regression curve fitting with GraphPad Prism 7.00 (GraphPad Software, La Jolla, CA).

Effects of IPO Stereochemistry on CYP4B1 Bioactivation

Metabolic incubations contained 25 pmol of purified rabbit CYP4B1 (Roellecke et al., 2016), 50 pmol of cytochrome P450 reductase, 25 pmol of cytochrome b5, 2.5 μg of DLPC, 100 U of catalase, 50 μg of superoxide dismutase, 10 mM NAL, and 10 mM NAC in 50 mM potassium phosphate buffer (KPi), pH 7.4, in a final volume of 100 μL . (*S*)-, (*R*)-, and racemic IPO were added to achieve a final concentration of 100 μM . The reaction was initiated by the addition of NADPH (1 mM final concentration) and allowed to progress for 30 minutes at 37°C. The reaction was quenched with an equal volume of acetonitrile containing 2 μM furafylline as the internal standard and centrifuged at 16,000g for 5 minutes. A supernatant aliquot (5 μL) was analyzed by UPLC-MS/MS on a Acquity UPLC connected to a Xevo TQ-S instrument (Waters, Milford, MA) in ESI+ mode with the following settings: capillary = 3.50 kV, cone = 40.0 V, source offset = 60.0 V, source temperature = 150°C, desolvation temperature = 350°C, cone gas flow = 150 L/hr, desolvation gas flow = 800 L/hr, and collision gas flow = 0.15 mL/min. Analytes were chromatographically separated using a Waters HSS T3 column (2.1 \times 100 mm, 1.8 μm) starting with 95% mobile phase A (0.1% formic acid in H_2O) and 5% mobile phase B (0.1% formic acid in acetonitrile) at a flow rate of 0.3 mL/min. After holding for 1 minute, B was increased linearly from 5% to 50% between 1 and 7 minutes, then from 50% to 100% between 7 and 7.5 minutes, and finally held at 100% between 7.5 and 9 minutes; total run time was 11 minutes following a 2-minute equilibration period. Under these conditions, IPO (all species), NAC/NAL adducts (all species), and furafylline were eluted at 5.32, 4.96, and 5.46 minutes, respectively, and were detected by multiple reaction monitoring (MRM) at m/z 151.07/95.04, 482.19/353.18, and 261.30/81.00, respectively. For IPO-NAC/NAL adduct quantification, an IPO-NAC/NAL adduct standard that we previously generated and characterized (Parkinson et al., 2016) was used. A 200 μM stock solution of this standard was prepared in 50 mM KPi, pH 7.4, and stored at -20°C . In duplicate, calibration standards were prepared using the stock solution diluted into a blank incubation matrix to obtain 10 concentrations spanning 0.024–12.5 μM . Metabolite analysis was performed with MassLynx V4.1 (Waters, Milford, MA) and quantitation was achieved by comparison of peak heights for the NAC/NAL adducts formed from the IPO enantiomers to the standard curve.

Purification and Characterization of 4-*Ipomeanol* Glucuronide Diastereomers

A racemic mixture of (*R,S*)-IPO-glucuronide diastereomers was synthesized as previously described (Parkinson et al., 2016). Semipreparative purification of (*R*)- and (*S*)-IPO-glucuronides was accomplished utilizing a Shimadzu HPLC system equipped with a Ultrasphere ODS column (250 \times 10 mm, 5 μm ; Beckman Coulter, Brea, CA) and UV/Vis detector. Baseline separation of the diastereomers was achieved by an isocratic elution (2.5 mL/min) with the mobile phase consisting of 82% 10 mM aqueous formic acid and 18% acetonitrile. Under these conditions, (*R*)-IPO-glucuronide and (*S*)-IPO-glucuronide were eluted at 7.9 and 8.7 minutes, respectively, and were detected at 254 nm. Each diastereomeric peak was collected in a round-bottom flask, and the organic solvent was evaporated. The aqueous components were frozen and lyophilized, and the respective white powders were characterized by NMR analysis (^1H , ^{13}C , and heteronuclear single quantum coherence) in acetonitrile- d_3 and by HRMS (Supplemental Figs. 2–9).

(*R*)-IPO-Glucuronide. ^1H NMR (500 MHz, CD_3CN): δ (ppm) 1.17 (d, J = 6.4 Hz, 3H), 1.73–1.90 (m, 2H), 2.82–2.98 (m, 2H), 3.08 (t, J = 8.5 Hz, 1H), 3.33 (t, J = 9.0 Hz, 1H), 3.45 (t, J = 9.3 Hz, 1H), 3.78 (d, J = 9.6 Hz, 1H), 3.81–3.87 (m, 1H), 4.36 (d, J = 7.7 Hz, 1H), 6.74 (s, 1H), 7.54 (s, 1H), 8.22 (s, 1H); ^{13}C NMR (125 MHz, CD_3CN): δ (ppm) 20.32, 32.04, 37.11, 72.62, 74.18 (2), 75.38, 76.91, 102.01, 109.21, 128.52, 145.52, 149.22, 170.72, 196.30; HRMS (ESI $^-$) calculated for $\text{C}_{15}\text{H}_{19}\text{O}_9$ [M-H] $^-$ 343.1024, found: 343.1025 (error 0.44 ppm).

(*S*)-IPO-Glucuronide. ^1H NMR (500 MHz, CD_3CN): δ (ppm) 1.22 (d, J = 6.2 Hz, 3H), 1.74–1.90 (m, 2H), 2.92 (td, J = 7.4, 6.9, 2.7 Hz, 2H), 3.13 (t, J = 8.5 Hz, 1H), 3.32 (t, J = 9.1 Hz, 1H), 3.45 (t, J = 9.4 Hz, 1H), 3.77 (d, J = 9.8 Hz, 1H), 3.78–3.85 (m, 1H), 4.38 (d, J = 7.8 Hz, 1H), 6.75 (s, 1H), 7.55 (s, 1H), 8.23 (s, 1H); ^{13}C NMR (125 MHz, CD_3CN): δ (ppm) 22.02, 31.68, 36.68, 72.51, 74.48, 75.18, 76.91, 77.06, 103.86, 109.24, 128.52, 145.64, 149.23, 170.72, 196.30; HRMS (ESI $^-$) calculated for $\text{C}_{15}\text{H}_{19}\text{O}_9$ [M-H] $^-$ 343.1023, found: 343.1024 (error 0.17 ppm).

UPLC-MS/MS Analysis

The chromatographic separation and quantification of IPO-glucuronide diastereomers was achieved using an Agilent 1290 Infinity liquid chromatograph (Agilent Technologies) coupled to an AB Sciex ABI 4000 triple quadrupole mass spectrometer (AB Sciex, Framingham, MA) equipped with an ESI probe or with the aforementioned Waters Acquity UPLC and Xevo TQ-S mass spectrometer. An Acquity UPLC HSS T3 column (100 \times 2.1 mm, 1.8 μm ; Waters) equipped with a precolumn C18 guard cartridge (Phenomenex, Torrance, CA) was used for the separation. The mobile phase consisted of (A) aqueous 10 mM formic acid and (B) 10 mM formic acid in acetonitrile at a flow rate of 0.350 mL/min. The total run time was 8.6 minutes with the following gradient elution: 5% B for 1 minute, linear gradient to 15% B between 1.0 and 1.5 minutes, held at 15% B until 3.0 minutes, linear increase to 40% B between 3.0 and 6.5 minutes, then re-equilibrated to initial conditions from 6.6 to 8.6 minutes. Under these conditions, (*R*)- and (*S*)-IPO-glucuronides were eluted at 4.9 and 5.1 minutes, respectively, and were detected by MRM at m/z 345/151. 4-MUG, which was used as the internal standard, was detected by MRM at m/z 353/177 and eluted at 4.8 minutes. The AB Sciex 4000 mass spectrometer was operated in positive-ion mode at 450°C with an ion spray voltage set at 4200 V, entrance potential of 10 V, and exit potential of 12 V. The curtain gas was set at 25, and ion source gas 1 and 2 at 35.

Stock solutions of each synthesized diastereomer were prepared in methanol at a 5-mM concentration and stored at -20°C . Standard-calibration stock solutions containing each diastereomer were prepared in 100 mM Tris, pH 7.5, to achieve a concentration range from 0.003 to 3.4 μM of (*R*)- and (*S*)-IPO-glucuronide. In duplicate, calibration standards were prepared by spiking 30 μL of the calibration stock solutions into 170 μL of a blank incubation matrix to achieve standard concentrations of 0.51–510 nM. Additionally, (4.5 nM), (75 nM), and (450 nM) quality control samples were prepared and run with each standard curve. The limit of quantitation was 0.51 nM, the lowest point on the standard curve.

Hydrolysis of Conjugates with β -Glucuronidase

A 1 μM solution containing both (*R*)- and (*S*)-IPO-glucuronide and a 1 μM solution of 4-MUG in sodium acetate, pH 5.0 (100 μL), were each incubated in the presence of 1000 U/mL of β -glucuronidase from *H. pomatia* at 37°C for 24 hours. The reactions were quenched by the addition of 10 μL of 15% ZnSO_4 (aq.), and the sample was centrifuged at 15,000g for 5 minutes. The supernatant was subsequently analyzed by the UPLC-MS/MS methods described earlier.

Recombinant UGT Screen

Thirteen recombinantly expressed UGT isoforms in baculovirus-infected insect cells (UGT1A1, 1A3, 1A4, 1A6, 1A7, 1A8, 1A9, 1A10, 2B4, 2B7, 2B10, 2B15, and 2B17) were purchased from Corning Life

Sciences (Tewksbury, MA). Incubations consisted of recombinant UGT enzyme (0.25 mg of total protein/mL), 100 mM Tris (pH 7.5), IPO (100 μ M), $MgCl_2$ (5 mM), alamethicin (10 μ g/mL), and UDPGA (5 mM) in a 200- μ L volume. Incubations were performed at 37°C for 60 minutes, and the reactions were quenched by the addition of 20 μ L of 15% $ZnSO_4$ (aq.), centrifuged at 15,000g, and injected onto the UPLC-MS/MS for analysis.

Microsomal UGT Activity

Human liver microsomes were prepared from eight adult donors of mixed gender by differential centrifugation according to previously published protocols (Lin et al., 2002). Human kidney microsomes (lot: 1310175, pool of 12, mixed gender) were purchased from Xenotech (Kansas City, MO). Microsomal incubations contained human liver or kidney microsomal protein (0.25 mg of total protein/mL), 100 mM Tris (pH 7.5), IPO (100 μ M), $MgCl_2$ (5 mM), alamethicin (10 μ g/mL) or 3-[(3-cholamidopropyl)dimethylammonio]-1-propanesulfonic acid (CHAPS; 0.5 mg/mL), UDPGA (5 mM), and one of the following: atazanavir (20 μ M), hecogenin (100 μ M), niflumic acid (2.5 μ M), or fluconazole (10 mM). All incubations contained 1% dimethylsulfoxide. Incubation mixtures were stored on ice for 15 minutes and preincubated in a 37°C water bath for 2 minutes followed by the addition of UDPGA (5 mM). Reactions were allowed to proceed for 60 minutes, at which time 20 μ L of 15% $ZnSO_4$ (aq.) was added to quench the reactions. The samples were centrifuged at 15,000g, and 20 μ L of the supernatant was injected onto the UPLC-MS/MS for analysis.

Results

Effect of IPO Stereochemistry on CYP4B1-Dependent Cytotoxicity. The cytotoxicity of (*S*)-, (*R*)-, and racemic IPO was assessed using a HepG2 cell proliferation (endpoint) assay 48 hours after dosing (Fig. 1A). No toxicity was observed in vehicle-treated wells as compared with wells with medium (data not shown). Control vector HepG2 cells showed no evidence of cytotoxicity from racemic IPO treatment up to 100 μ M, indicating the absence or low expression of any endogenous IPO-bioactivating enzymes that could cause toxicity. Rabbit CYP4B1-expressing HepG2 cells exposed to (*S*)-, (*R*)-, and racemic IPO displayed nearly overlapping dose-cytotoxicity-response curves, which generated LD_{50} values of 5.8, 5.7, and 5.7 μ M, respectively. Almost identical results were obtained with the optimized human CYP4B1 “P+12” enzyme, with observed LD_{50} values of 5.3, 6.1, and 5.4 μ M for (*S*)-, (*R*)-, and racemic IPO, respectively (Fig. 1B). In the CYP4B1-expressing HepG2

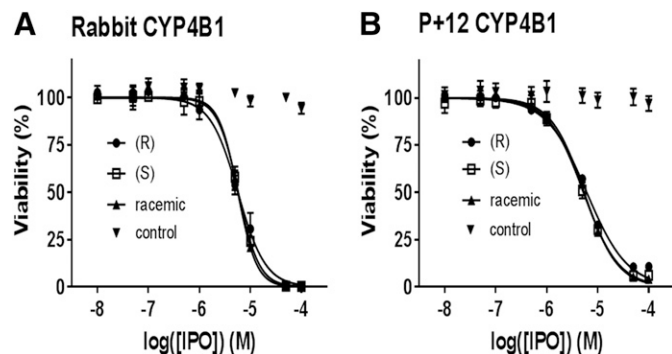


Fig. 1. Cytotoxicity dose-response curves in HepG2 cells transfected with rabbit CYP4B1 (A) and human P+12 CYP4B1 (B) from treatment with (*S*)-, (*R*)-, racemic IPO, and control HepG2 cells treated with racemic IPO. Data shown are the mean \pm S.D. from triplicate replicates.

cells, >99% cell death was observed with all compounds at a dose of 50 μ M.

Effect of IPO Stereochemistry on CYP4B1-Dependent Substrate Depletion and NAC/NAL Adduct Formation. To determine the effect of IPO enantiomers on CYP4B1-mediated substrate consumption and reactive intermediate formation, metabolism of the substrates in reconstituted systems of purified rabbit CYP4B1 was investigated. IPO depletion, in 30-minute incubations with 25 pmol of CYP4B1, showed no enantiomer preference (Fig. 2A), with averages of 18.8%, 18.1%, and 18.1% consumed substrate for (*S*)-, (*R*)-, and racemic IPO, respectively. In probing IPO furan oxidation by trapping the reactive intermediate with NAC/NAL, no enantiomer preference was observed (Fig. 2B). Quantification yielded average adduct formation rates of 28.3, 28.4, and 32.2 pmol/pmol of P450/30 minutes for (*S*)-, (*R*)-, and racemic IPO, respectively, thus demonstrating no stereochemical differences in adduct formation by CYP4B1. Additionally, no IPO enantioselectivity was observed in the reconstituted systems with regard to CYP4B1-dependent substrate depletion or NAC/NAL adduct formation.

Identification and Characterization of (*R*)- and (*S*)-IPO-Glucuronide Diastereomers. (*R,S*)-IPO-glucuronide diastereomers were synthesized as previously described (Parkinson et al., 2016) and separated with baseline resolution using a UPLC-MS/MS method (Fig. 3A). The detection of 4-MUG (Fig. 3B) was also achieved using the same analytical method. Solutions (1 μ M) of the glucuronides and 4-MUG were each incubated in the presence of β -glucuronidase from *H. pomatia*. In each case, all glucuronides were successfully cleaved with >99% efficiency (Fig. 3, C and D). To confirm the absolute configuration of each glucuronide diastereomer, (*R*)- and (*S*)-IPO were initially synthesized by a modified procedure described previously (Alvarez-Diez and Zheng, 2004). Each enantiomer was subsequently incubated with human liver microsomes (HLMs) to form their respective glucuronide (Fig. 4, B and C). When compared with an incubation with racemic IPO (Fig. 4A), (*R*)-IPO-glucuronide was identified as the first peak (4.86 minutes) and (*S*)-IPO-glucuronide as the second eluting peak (5.18 minutes). To further confirm the identity of the glucuronide(s), 100 μ M IPO was incubated with human liver microsomes in the absence of UDGPA (Fig. 4D).

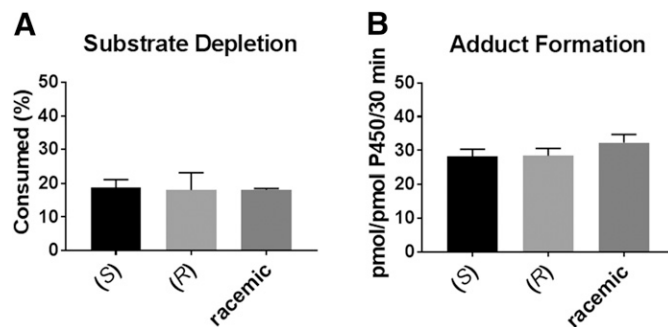


Fig. 2. Comparison of substrate depletion (A) and quantification of NAC/NAL adduct formation (B) in reconstituted CYP4B1 incubations after 30 minutes with 25 pmol of P450 and 100 μ M IPO substrates. Data shown are the mean \pm S.D. from triplicate replicates.

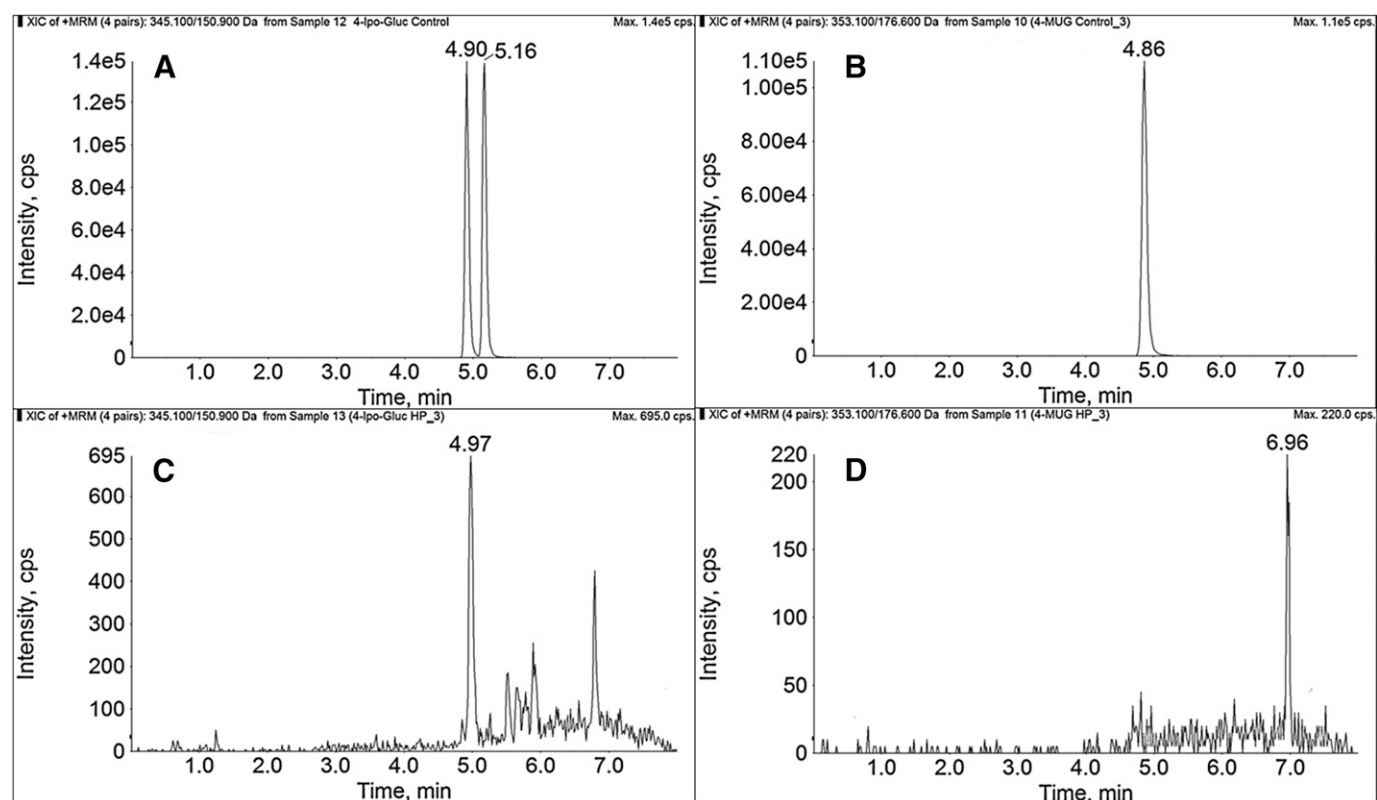


Fig. 3. Chromatographic separation of (*R,S*)-IPO-glucuronide (A) and 4-methylumbelliferone glucuronide (B) by UPLC-MS/MS. Incubation of $1\ \mu\text{M}$ (*R,S*)-IPO-glucuronide (C) and $1\ \mu\text{M}$ 4-methylumbelliferone glucuronide (D) in the presence of *H. pomatia* (1000 U/mL) in potassium acetate, pH 5, for 24 hours at 37°C . XIC, Extracted Ion Chromatogram.

Optimization of Microsomal Incubation Conditions: Effects of Buffer, pH, Alamethicin, and CHAPS on Specific Activity and Diastereoselectivity of IPO Glucuronidation.

Previously, we compared microsomal glucuronidation of racemic IPO across a number of species, including humans, where formation rates were low relative to experimental animals (Parkinson et al., 2016). Therefore, for the current studies, we used new lots of commercially available liver and kidney microsomes, used higher microsomal protein and substrate concentrations, and performed glucuronide analysis on more-sensitive MS instruments. With these modifications in place, we first evaluated the specific activity and diastereoselectivity of glucuronidation in human liver microsomal incubations containing either 100 mM KPi (pH 6.0–8.0) or 100 mM Tris (pH 7.0–8.5 at 37°C), 100 μM IPO, 5 mM MgCl_2 , 10 $\mu\text{g}/\text{mL}$ alamethicin, and 5 mM UDPGA (Fig. 5). The MgCl_2 , alamethicin, and UDPGA concentrations were mirrored based on the previous work conducted by Walsky et al. (2012). At pH 7.5, there was no dramatic difference in specific activity using either KPi or Tris, although the diastereomeric ratio tended to favor (*R*)-IPO-glucuronide more using Tris buffer. Specific activity increased as the pH increased from 6.0 to 8.0 in KPi, but with little diastereoselectivity at the higher pHs. Additionally, we assessed the effect of either the detergent CHAPS (Lett et al., 1992) or pore-forming reagent alamethicin on IPO glucuronidation in human liver microsomes (data not shown). These incubations contained 100 mM Tris (pH 7.5) at 37°C , 100 μM IPO, 5 mM MgCl_2 , 10 $\mu\text{g}/\text{mL}$ alamethicin or 0.5 mg/mL CHAPS, and 5 mM UDPGA. There was a pronounced difference between alamethicin and CHAPS

under these conditions. Whereas diastereoselectivity was retained in each case, the specific activity was dramatically increased when alamethicin was used. Based on these optimization efforts, all further metabolic incubations were carried out in Tris pH 7.5 buffer and with the inclusion of alamethicin.

Recombinant UGT Screen. To identify the specific isoform(s) responsible for IPO glucuronidation, a commercially available panel of 13 UGT recombinant enzymes was investigated. Screening with 0.25 mg/mL of each recombinant UGT (rUGT) and substrate (100 μM) indicated that UGT1A9, UGT2B7, and UGT2B15 were the predominant isoforms catalyzing glucuronidation of IPO (Fig. 6). UGT1A9 and UGT2B7 formed (*R*)-IPO-glucuronide preferentially, whereas UGT2B15 was selective for formation of (*S*)-IPO-glucuronide. The specific activities for formation of (*R*)- and (*S*)-IPO-glucuronide and the respective diastereomeric ratios in the recombinant UGT enzymes and microsomes are provided in Table 1.

Human Liver and Kidney Microsomal Incubations. To better evaluate which UGT isoforms dominate microsomal glucuronidation, racemic IPO (100 μM) was incubated with human liver microsomes in the presence of selective UGT inhibitors: 10 mM atazanavir (UGT1A1) (Zhang et al., 2005), 100 μM hecogenin (1A4) (Uchaipichat et al., 2006a), 2.5 μM niflumic acid (1A9) (Miners et al., 2011), and 10 mM fluconazole (2B7) (Uchaipichat et al., 2006b; Fang et al., 2013) (Table 2). Glucuronidation was inhibited by fluconazole (60%–65%) and marginally inhibited by niflumic acid (16%–28%), hecogenin (20%–22%), and atazanavir [26% inhibition of

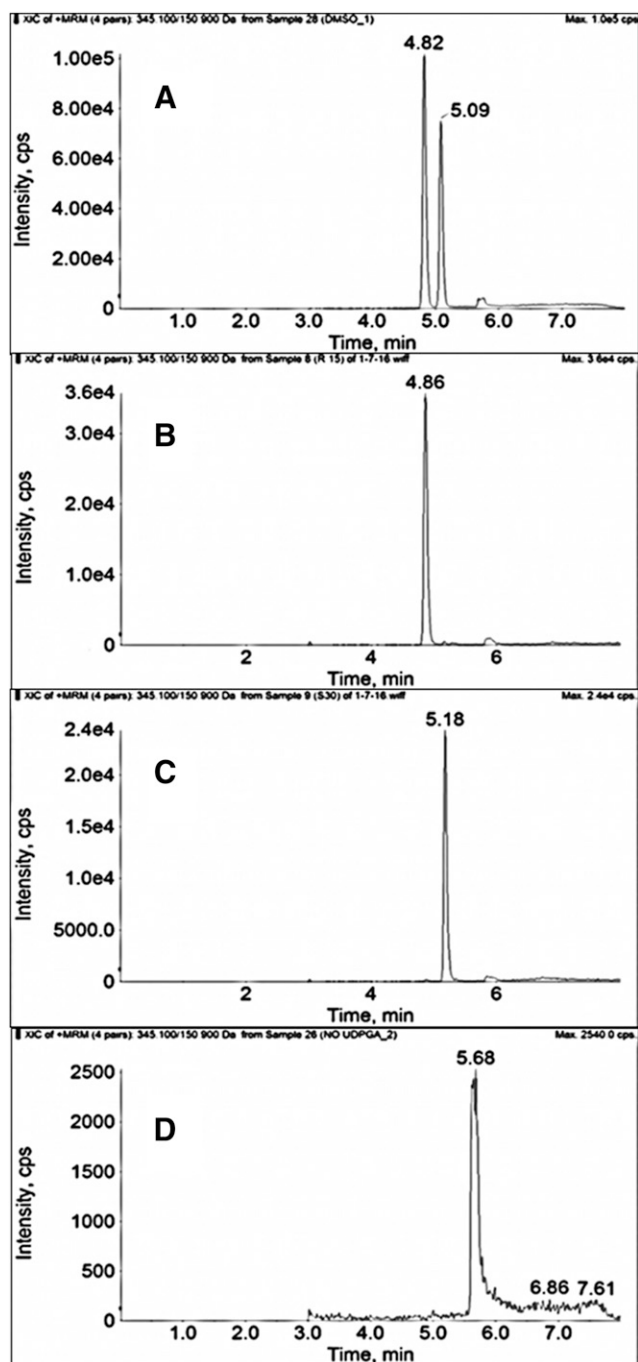


Fig. 4. Representative chromatographic traces of (*R*)- and (*S*)-IPO-glucuronides. (A) Incubation of 100 μ M IPO in Tris buffer (pH 7.5), 10 μ g/mL alamethicin, 5 mM MgCl₂, and 5 mM UDPGA with 0.25 mg/mL human liver microsomes. Incubation of 100 μ M (*R*)-IPO (B) and (*S*)-IPO (C) in human liver microsomes. (D) Incubation of 100 μ M racemic IPO with human liver microsomes in the absence of UDPGA.

(*R*)-IPO-glucuronide]. These data suggest that UGT2B7 dominates human liver microsomal glucuronidation of IPO, although we cannot preclude contributions from other UGT enzymes, such as UGT2B4, which is a major UGT isoform in human liver microsomes. Because UGT2B7 and UGT2B15 exhibit opposite diastereoselectivities, the net effect is that human liver microsomes display little diastereoselectivity for IPO glucuronidation. In contrast, in human kidney

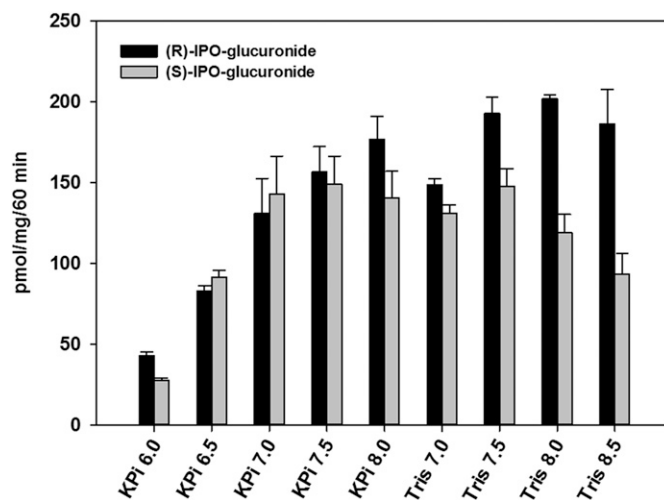


Fig. 5. Diastereoselective glucuronidation of racemic IPO in human liver microsomes. Incubations were conducted with 100 μ M IPO in potassium phosphate buffer (pH 6.0–8.0) and Tris buffer (pH 7.0–8.5) with 0.25 mg/mL microsomal protein, 10 μ g/mL alamethicin, 5 mM MgCl₂, and 5 mM UDPGA for 60 minutes at 37°C. The Tris pH reflects the actual pH at 37°C. Results are reported as the specific activity mean \pm S.D. of three determinations.

microsomes, niflumic acid was a strong inhibitor (68%–76%) of human kidney microsomal glucuronidation, suggesting a dominant role for UGT1A9 in this tissue. Renal glucuronidation of IPO was also similarly inhibited by fluconazole (36%–58%) compared with hepatic glucuronidation, providing evidence for a contribution by UGT2B7 (Table 2).

Discussion

IPO occupies an important position in the history of extrahepatic P450-dependent toxicology (Gram, 1997). However, despite almost 50 years of research on this topic, and interest in the compound for GDEPT, no prior data exist on the influence of stereochemistry on the protoxin's bioactivation or its inactivation via glucuronidation. Given that the location of the chiral center in IPO is at C-4, one could hypothesize that glucuronidation of the IPO enantiomers would be impacted more than bioactivation, which occurs on the furan ring that is distant from C-4. In fact, for CYP4B1, regardless of whether the source of the enzyme is the native rabbit sequence or the optimized human (P+12) sequence, the cytotoxic effects of IPO enantiomers in transfected HepG2 cells are the same. Detailed analysis using purified reconstituted rabbit CYP4B1 further confirmed that depletion of (*R*)-IPO and (*S*)-IPO in purified enzyme incubations as well as the flux to the reactive enedial intermediate were enantiomer independent. In the aggregate, it is clear that the IPO racemate is an appropriate choice for future work on the development of a CYP4B1-dependent suicide gene system.

Enantioselective glucuronidation of drugs has been recognized since the early 1980s when the benzodiazepine oxazepam was shown to be preferentially glucuronidated to *S*-oxazepam in humans (Seideman et al., 1981). Subsequently, many additional drugs and hydroxylated metabolites were shown to undergo stereoselective glucuronidation (Miners and Mackenzie, 1991) that reflected preferential metabolism by certain UGT isoforms (Court, 2005; Rowland et al., 2013). To pursue

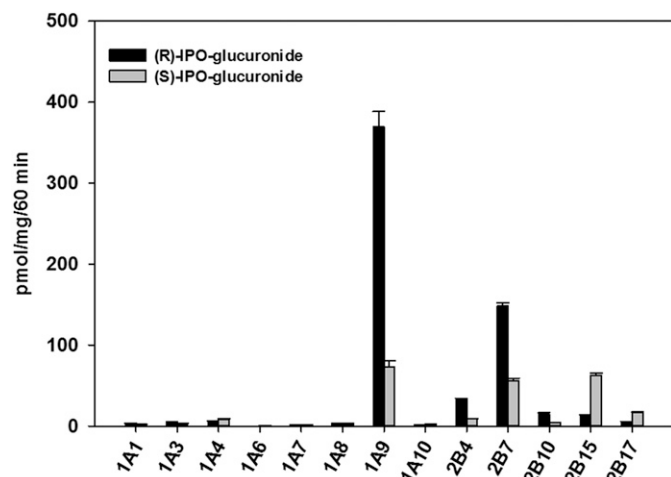


Fig. 6. (*R*)- and (*S*)-IPO-glucuronide formation utilizing a panel of 13 recombinantly expressed UGT isoforms. Racemic IPO (100 μ M) was incubated with rUGT (0.25 mg of total protein/mL), alamethicin (10 μ g/mL), $MgCl_2$ (5 mM), and UDPGA (5 mM) for 60 minutes at 37°C. Results are reported as the specific activity mean \pm S.D. of three determinations.

questions related to the stereochemistry of IPO glucuronidation, we took the approach of quantifying the diastereoselectivity of the enzymatic reactions. This was accessible once chromatographic conditions were identified that resolved the diastereomers. Independent chemical synthesis of the diastereomers and microsomal glucuronidation reactions with the individual IPO enantiomers enabled unambiguous assignment of product diastereoselectivity. Optimization of buffer composition, pH, and inclusion of alamethicin in metabolic reactions, together with other assay improvements facilitated analyte detection and provided a robust method for determining the stereochemistry of IPO formation and evaluating the specific isoforms that likely contribute to this potential clearance pathway. The latter is important because, if IPO glucuronidation is important in humans *in vivo*, as it appears to be in rodents (Statham et al., 1982), genetic variability in UGT activity needs to be evaluated in terms of the risk for hepatotoxicity in humans treated with IPO.

Peak plasma concentrations of IPO from previous clinical studies were about 100 μ M (Rowinsky et al., 1993), and this concentration (total C_{max}) was used in all *in vitro* experiments described. Performing the rUGT, HLM, and human kidney microsome incubations at the clinically reported IPO C_{max} is optimal for generating data that have the likeliest chance of translating to the clinic. Therefore, all *in vitro* experiments were only conducted with the most physiologically relevant IPO concentration. Screening of a panel of 13 recombinantly

expressed UGTs identified UGT1A9, UGT2B7, and UGT 2B15 as the dominant isoforms when incubations were performed with IPO. Notably, however, incubations with human liver microsomes in the presence of selective UGT inhibitors suggested that UGT1A9 and UGT2B7 are the more likely contributors *in vivo*. Despite the high catalytic activity of recombinant UGT1A9, this isoform may not be a prominent contributor to human liver IPO glucuronidation because it is a minor constituent (6%–9%) of the total UGT pool (Margaillan et al., 2015). Additionally, recent evidence suggests the expression levels of UGT1A9 in human kidney microsomes are 3.1-fold higher than HLMs and may account for the marginal inhibition by niflumic acid in HLMs (Nakamura et al., 2016). Moreover, UGT1A9 exhibits pronounced selectivity for glucuronidation of (*R*)-IPO over (*S*)-IPO, but this is not recapitulated in the diastereoselectivity found in human liver microsomes. This observation further undermines a major contribution of UGT1A9 to IPO glucuronidation in human liver. In contrast, UGT1A9 is clearly the major contributor to human kidney glucuronidation on the basis of both diastereoselectivity and chemical inhibition studies. Human renal glucuronidation has been reasonably well characterized (Knights et al., 2013) and is important for drugs such as propofol and mycophenolic acid (Gill et al., 2012; Knights et al., 2016). Although polymorphisms are present in all UGT enzymes, high-frequency deleterious variants that impact the clearance of therapeutic drugs are limited largely to UGT1A1, UGT2B15, UGT2B17, and, to a lesser extent, UGT1A9 (Stingl et al., 2014). Whereas UGT1A1 and UGT2B17 appear to have minimal roles in the glucuronidation of IPO, UGT2B15 is probably a contributor based on the rUGT phenotypic screen. Since the common mutation, D85Y, in UGT2B15 is a major determinant of oxazepam clearance *in vivo* (He et al., 2009), it would be interesting to determine if this mutation is a risk factor for IPO-induced liver toxicity in humans. The opposite holds true for UGT1A9 polymorphisms, which are attributed to increased protein expression levels and, subsequently, higher clearance of UGT1A9 substrates, such as mycophenolic acid (Baldelli et al., 2007).

In summary, we demonstrated that IPO stereochemistry does not affect CYP4B1-mediated bioactivation of this protoxin but does influence product diastereoselectivity generated from human liver and kidney UGTs. The major enzymes capable of racemic IPO glucuronidation are UGT1A9, UGT2B7, and UGT2B15. Major isoform-dependent differences in product diastereoselectivity together with chemical inhibition experiments help identify UGT1A9 and members of the UGT2B family as the likely contributors to human hepatic glucuronidation of IPO. Therefore, beyond common genetic polymorphisms in UGT2B15, we speculate that drug-drug interactions with concomitantly administered UGT2B

TABLE 1

Specific activities for formation of (*R*)- and (*S*)-IPO-glucuronide and the respective diastereomeric ratios by recombinant UGT enzymes and microsomal preparations

Specific activity (pmol/mg per 60 minutes) expressed as the mean \pm S.D. of three replicates.

	Enzyme Source							
	rUGT1A9	rUGT2B4	rUGT2B7	rUGT2B10	rUGT2B15	rUGT2B17	HLM	HKM
(<i>R</i>)-IPO-glucuronide	369 \pm 18.8	34 \pm 0.49	148 \pm 3.6	15 \pm 1.6	13 \pm 0.87	5 \pm 0.39	303 \pm 8.5	383 \pm 12
(<i>S</i>)-IPO-glucuronide	73 \pm 7.5	8.7 \pm 0.87	56 \pm 2.8	4 \pm 0.39	63 \pm 2.6	17 \pm 0.42	227 \pm 7.9	104 \pm 2.5
Diastereomeric ratio (<i>R/S</i>)	5.1	3.9	2.6	3.8	0.21	0.29	1.3	3.7

HKM, human kidney microsome.

TABLE 2

Chemical inhibition of (*R*)- and (*S*)-IPO glucuronidation in human liver and kidney microsomes

Values represent the percentage of glucuronide remaining relative to a normalized control (100% glucuronide remaining in the absence of inhibitor) expressed as the mean \pm S.D. of three replicates.

	(<i>R</i>)-IPO-glucuronide	(<i>S</i>)-IPO-glucuronide
HLM		
No inhibitor	100 \pm 8 ^a	100 \pm 3 ^b
20 μ M atazanavir	74 \pm 1	94 \pm 3
100 μ M hecogenin	78 \pm 15	80 \pm 9
2.5 μ M niflumic acid	72 \pm 5	84 \pm 10
10 mM fluconazole	35 \pm 5	40 \pm 2
HKM		
No inhibitor	100 \pm 3 ^c	100 \pm 2 ^d
2.5 μ M niflumic acid	24 \pm 8	32 \pm 6
10 mM fluconazole	64 \pm 10	42 \pm 4

HKM, human kidney microsome.

^aSpecific activities of (*R*)-IPO-glucuronide and (*S*)-IPO-glucuronide formation in HLM: 303 \pm 8 pmol/mg/60 minutes.

^bSpecific activities of (*R*)-IPO-glucuronide and (*S*)-IPO-glucuronide formation in HLM: 227 \pm 8 pmol/mg/60 minutes.

^cSpecific activities of (*R*)-IPO-glucuronide and (*S*)-IPO-glucuronide formation in HKM: 383 \pm 12 pmol/mg/60 minutes.

^dSpecific activities of (*R*)-IPO-glucuronide and (*S*)-IPO-glucuronide formation in HKM: 104 \pm 2 pmol/mg/60 minutes.

substrates might affect the overall clearance of racemic IPO in pharmacological gene therapy. Future work in this area should also focus on delineating the relative importance of other phase II detoxifying enzymes to IPO metabolism in humans.

Acknowledgments

We thank J. Scott Edgar for his assistance with high-resolution mass spectrometry.

Authorship Contributions

Participated in research design: Teitelbaum, McDonald, Kowalski, Parkinson, Hanenberg, Rettie.

Conducted experiments: Teitelbaum, McDonald Kowalski, Whittington, Roellecke, Wiek, Scian.

Performed data analysis: Teitelbaum, McDonald, Kowalski, Scian.

Wrote or contributed to the writing of the manuscript: Teitelbaum, Kowalski, Rettie.

References

- Alvarez-Diez TM and Zheng J (2004) Mechanism-based inactivation of cytochrome P450 3A4 by 4-ipomeanol. *Chem Res Toxicol* **17**:150–157.
- Baer BR, Rettie AE, and Henne KR (2005) Bioactivation of 4-ipomeanol by CYP4B1: adduct characterization and evidence for an enedial intermediate. *Chem Res Toxicol* **18**:855–864.
- Baldelli S, Merlini S, Perico N, Nicastrì A, Cortinovis M, Gotti E, Remuzzi G, and Cattaneo D (2007) C-440T/T-331C polymorphisms in the UGT1A9 gene affect the pharmacokinetics of mycophenolic acid in kidney transplantation. *Pharmacogenomics* **8**:1127–1141.
- Boyd MR, Wilson BJ, and Harris TM (1972) Confirmation by chemical synthesis of the structure of 4-ipomeanol, a lung-toxic metabolite of the sweet potato, *Ipomoea batatas*. *Nat New Biol* **236**:158–159.
- Court MH (2005) Isoform-selective probe substrates for in vitro studies of human UDP-glucuronosyltransferases. *Methods Enzymol* **400**:104–116.
- Devereux TR, Jones KG, Bend JR, Fouts JR, Statham CN, and Boyd MR (1982) In vitro metabolic activation of the pulmonary toxin, 4-ipomeanol, in nonciliated bronchiolar epithelial (Clara) and alveolar type II cells isolated from rabbit lung. *J Pharmacol Exp Ther* **220**:223–227.
- Dutcher JS and Boyd MR (1979) Species and strain differences in target organ alkylation and toxicity by 4-ipomeanol. Predictive value of covalent binding in studies of target organ toxicities by reactive metabolites. *Biochem Pharmacol* **28**:3367–3372.
- Falzon M, McMahon JB, Schuller HM, and Boyd MR (1986) Metabolic activation and cytotoxicity of 4-ipomeanol in human non-small cell lung cancer lines. *Cancer Res* **46**:3484–3489.
- Fang ZZ, He RR, Cao YF, Tanaka N, Jiang C, Krausz KW, Qi Y, Dong PP, Ai CZ, Sun XY, et al. (2013) A model of in vitro UDP-glucuronosyltransferase inhibition by bile acids predicts possible metabolic disorders. *J Lipid Res* **54**:3334–3344.
- Frank S, Steffens S, Fischer U, Tolkko A, Rainov NG, and Kramm CM (2002) Differential cytotoxicity and bystander effect of the rabbit cytochrome P450 4B1

- enzyme gene by two different prodrugs: implications for pharmacogene therapy. *Cancer Gene Ther* **9**:178–188.
- Gill KL, Houston JB, and Galetin A (2012) Characterization of in vitro glucuronidation clearance of a range of drugs in human kidney microsomes: comparison with liver and intestinal glucuronidation and impact of albumin. *Drug Metab Dispos* **40**:825–835.
- Gram TE (1997) Chemically reactive intermediates and pulmonary xenobiotic toxicity. *Pharmacol Rev* **49**:297–341.
- He X, Hesse LM, Hazarika S, Masse G, Hartzat JS, Greenblatt DJ, and Court MH (2009) Evidence for oxazepam as an in vivo probe of UGT2B15: oxazepam clearance is reduced by UGT2B15 D85Y polymorphism but unaffected by UGT2B17 deletion. *Br J Clin Pharmacol* **68**:721–730.
- Hsu H, Rainov NG, Quinones A, Eling DJ, Sakamoto KM, and Spear MA (2003) Combined radiation and cytochrome CYP4B1/4-ipomeanol gene therapy using the EGR1 promoter. *Anticancer Res* **23** (3B):2723–2728.
- Jang SJ, Kang JH, Lee TS, Kim SJ, Kim KI, Lee YJ, Cheon GJ, Choi CW, and Lim SM (2010) Prodrug-activating gene therapy with rabbit cytochrome P450 4B1/4-ipomeanol or 2-aminoanthracene system in glioma cells. *Nucl Med Mol Imaging* **44**:193–198.
- Kasturi VK, Dearing MP, Piscitelli SC, Russell EK, Sladek GG, O'Neil K, Turner GA, Morton TL, Christian MC, Johnson BE, et al. (1998) Phase I study of a five-day dose schedule of 4-ipomeanol in patients with non-small cell lung cancer. *Clin Cancer Res* **4**:2095–2102.
- Knights KM, Rowland A, and Miners JO (2013) Renal drug metabolism in humans: the potential for drug-endobiotic interactions involving cytochrome P450 (CYP) and UDP-glucuronosyltransferase (UGT). *Br J Clin Pharmacol* **76**:587–602.
- Knights KM, Spencer SM, Fallon JK, Chau N, Smith PC, and Miners JO (2016) Scaling factors for the in vitro-in vivo extrapolation (IV-IVE) of renal drug and xenobiotic glucuronidation clearance. *Br J Clin Pharmacol* **81**:1153–1164.
- Lett E, Kriszt W, de Sandro V, Ducrotot G, and Richert L (1992) Optimal detergent activation of rat liver microsomal UDP-glucuronosyl transferases toward morphine and 1-naphthol: contribution to induction and latency studies. *Biochem Pharmacol* **43**:1649–1653.
- Lin YS, Dowling AL, Quigley SD, Farin FM, Zhang J, Lamba J, Schuetz EG, and Thummel KE (2002) Co-regulation of CYP3A4 and CYP3A5 and contribution to hepatic and intestinal midazolam metabolism. *Mol Pharmacol* **62**:162–172.
- Margaillan G, Rouleau M, Klein K, Fallon JK, Caron P, Villeneuve L, Smith PC, Zanger UM, and Guillemette C (2015) Multiplexed targeted quantitative proteomics predicts hepatic glucuronidation potential. *Drug Metab Dispos* **43**:1331–1335.
- McLemore TL, Coudert BP, and Adelberg S (1988) Metabolic activation of 4-ipomeanol by human pulmonary carcinoma cells propagated in vitro and intrabronchially in nude mice. *Clin Res* **36**:498A.
- Miners JO, Bowalgha K, Elliot DJ, Baranczewski P, and Knights KM (2011) Characterization of niflumic acid as a selective inhibitor of human liver microsomal UDP-glucuronosyltransferase 1A9: application to the reaction phenotyping of acetaminophen glucuronidation. *Drug Metab Dispos* **39**:644–652.
- Miners JO and Mackenzie PI (1991) Drug glucuronidation in humans. *Pharmacol Ther* **51**:347–369.
- Mohr L, Rainov NG, Mohr UG, and Wands JR (2000) Rabbit cytochrome P450 4B1: a novel prodrug activating gene for pharmacogene therapy of hepatocellular carcinoma. *Cancer Gene Ther* **7**:1008–1014.
- Moon BS, Jang SJ, Kim SJ, Lee TS, Chi DY, Lee BC, Kang JH, and Kim SE (2013) Synthesis and evaluation of a 18F-labeled 4-ipomeanol as an imaging agent for CYP4B1 gene prodrug activation therapy. *Cancer Biother Radiopharm* **28**:588–597.
- Nakamura K, Hirayama-Kurogi M, Ito S, Kuno T, Yoneyama T, Obuchi W, Terasaki T, and Ohtsuki S (2016) Large-scale multiplex absolute protein quantification of drug-metabolizing enzymes and transporters in human intestine, liver, and kidney microsomes by SWATH-MS: comparison with MRM/SRM and HR-MRM/PRM. *Proteomics* **16**:2106–2117.
- Parkinson OT, Teitelbaum AM, Whittington D, Kelly EJ, and Rettie AE (2016) Species differences in microsomal oxidation and glucuronidation of 4-ipomeanol: relationship to target organ toxicity. *Drug Metab Dispos* **44**:1598–1602.
- Rainov NG, Dobberstein KU, Sena-Esteves M, Herrlinger U, Kramm CM, Philpot RM, Hilton J, Chiocca EA, and Breakfield XO (1998a) New prodrug activation gene therapy for cancer using cytochrome P450 4B1 and 2-aminoanthracene/4-ipomeanol. *Hum Gene Ther* **9**:1261–1273.
- Rainov NG, Sena-Esteves M, Fraefel C, Dobberstein KU, Chiocca EA, and Breakfield XO (1998b) A chimeric fusion protein of cytochrome CYP4B1 and green fluorescent protein for detection of pro-drug activating gene delivery and for gene therapy in malignant glioma. *Adv Exp Med Biol* **451**:393–403.
- Roellecke K, Virts EL, Einholz R, Edson KZ, Altwater B, Rossig C, von Laer D, Scheckenbach K, Wagenmann M, Reinhardt D, et al. (2016) Optimized human CYP4B1 in combination with the alkylator prodrug 4-ipomeanol serves as a novel suicide gene system for adoptive T-cell therapies. *Gene Ther* **23**:615–626.
- Rowinsky EK, Nee DA, Ettinger DS, Christian MC, Lubejko BG, Fishman EK, Sartorius SE, Boyd MR, and Donehower RC (1993) Phase I and pharmacological study of the pulmonary cytotoxin 4-ipomeanol on a single dose schedule in lung cancer patients: hepatotoxicity is dose limiting in humans. *Cancer Res* **53**:1794–1801.
- Rowland A, Miners JO, and Mackenzie PI (2013) The UDP-glucuronosyltransferases: their role in drug metabolism and detoxification. *Int J Biochem Cell Biol* **45**:1121–1132.
- Schmidt EM, Wiek C, Parkinson OT, Roellecke K, Freund M, Gombert M, Lottmann N, Steward CA, Kramm CM, Yarov-Yarovsky V, et al. (2015) Characterization of an additional splice acceptor site introduced into CYP4B1 in hominoidae during evolution. *PLoS One* **10**:e0137110.
- Seideman P, Ericsson O, Grönningsson K, and von Bahr C (1981) Effect of pentobarbital on the formation of diastereomeric oxazepam glucuronides in man: analysis by high performance liquid chromatography. *Acta Pharmacol Toxicol (Copenh)* **49**:200–204.

- Smith AC, Barrett D, Stedham MA, el-Hawari M, Kastello MD, Grieshaber CK, and Boyd MR (1987) Preclinical toxicology studies of 4-ipomeanol: a novel candidate for clinical evaluation in lung cancer. *Cancer Treat Rep* **71**: 1157–1164.
- Smith PB, Tiano HF, Nesnow S, Boyd MR, Philpot RM, and Langenbach R (1995) 4-Ipomeanol and 2-aminoanthracene cytotoxicity in C3H/10T1/2 cells expressing rabbit cytochrome P450 4B1. *Biochem Pharmacol* **50**:1567–1575.
- Statham CN, Dutcher JS, Kim SH, and Boyd MR (1982) Ipomeanol 4-glucuronide, a major urinary metabolite of 4-ipomeanol in the rat. *Drug Metab Dispos* **10**: 264–267.
- Steffens S, Frank S, Fischer U, Heuser C, Meyer KL, Dobberstein KU, Rainov NG, and Kramm CM (2000) Enhanced green fluorescent protein fusion proteins of herpes simplex virus type 1 thymidine kinase and cytochrome P450 4B1: applications for prodrug-activating gene therapy. *Cancer Gene Ther* **7**: 806–812.
- Stingl JC, Bartels H, Viviani R, Lehmann ML, and Brockmüller J (2014) Relevance of UDP-glucuronosyltransferase polymorphisms for drug dosing: a quantitative systematic review. *Pharmacol Ther* **141**:92–116.
- Uchaipichat V, Mackenzie PI, Elliot DJ, and Miners JO (2006a) Selectivity of substrate (trifluoperazine) and inhibitor (amitriptyline, androsterone, canrenoic acid, hecogenin, phenylbutazone, quinidine, quinine, and sulfapyrazone) “probes” for human udp-glucuronosyltransferases. *Drug Metab Dispos* **34**:449–456.
- Uchaipichat V, Winner LK, Mackenzie PI, Elliot DJ, Williams JA, and Miners JO (2006b) Quantitative prediction of in vivo inhibitory interactions involving glucuronidated drugs from in vitro data: the effect of fluconazole on zidovudine glucuronidation. *Br J Clin Pharmacol* **61**:427–439.
- Verschoye RD, Philpot RM, Wolf CR, and Dinsdale D (1993) CYP4B1 activates 4-ipomeanol in rat lung. *Toxicol Appl Pharmacol* **123**:193–198.
- Walsky RL, Bauman JN, Bourcier K, Giddens G, Lapham K, Negahban A, Ryder TF, Obach RS, Hyland R, and Goosen TC (2012) Optimized assays for human UDP-glucuronosyltransferase (UGT) activities: altered alamethicin concentration and utility to screen for UGT inhibitors. *Drug Metab Dispos* **40**:1051–1065.
- Wiek C, Schmidt EM, Roellecke K, Freund M, Nakano M, Kelly EJ, Kaisers W, Yarov-Yarovoy V, Kramm CM, Rettie AE, et al. (2015) Identification of amino acid determinants in CYP4B1 for optimal catalytic processing of 4-ipomeanol. *Biochem J* **465**:103–114.
- Wilson BJ and Burka LT (1979) Toxicity of novel sesquiterpenoids from the stressed sweet potato (*Ipomoea batatas*). *Food Cosmet Toxicol* **17**:353–355.
- Zhang D, Chando TJ, Everett DW, Patten CJ, Dehal SS, and Humphreys WG (2005) In vitro inhibition of UDP glucuronosyltransferases by atazanavir and other HIV protease inhibitors and the relationship of this property to in vivo bilirubin glucuronidation. *Drug Metab Dispos* **33**:1729–1739.

Address correspondence to: Aaron M. Teitelbaum, Drug Metabolism and Pharmacokinetics, Boehringer Ingelheim, Pharmaceuticals, Inc., 900 Ridgebury Road, Ridgefield, CT 06877-0368. E-mail: aaron.teitelbaum@boehringer-ingelheim.com

TITLE PAGE

**Influence of Stereochemistry on the Bioactivation and Glucuronidation of
4-Ipomeanol**

Aaron M. Teitelbaum, Matthew G. McDonald, John P. Kowalski, Oliver T. Parkinson,
Michele Scian, Dale Whittington, Katharina Roellecke, Helmut Hanenberg, Constanze
Wiek, and Allan E. Rettie

Department of Medicinal Chemistry, School of Pharmacy, University of Washington,
Seattle, WA 98105, USA (A.M.T., M.G.M., J.P.K., O.T.P., M.S., D.W., A.E.R.);

Department of Otorhinolaryngology and Head/Neck Surgery, Heinrich-Heine University,
40225 Düsseldorf, Germany (K.R., H.H., C.W.); Department of Pediatrics III, University
Children's Hospital Essen, University of Duisburg-Essen, 45122 Essen, Germany (H.H.)

Table of Contents

Supplemental Figure 1: Synthetic Scheme for of (*R*)- and (*S*)-4-Ipomeanol

Supplemental Figure 2: ^1H NMR spectrum of (*R*)-IPO-glucuronide

Supplemental Figure 3: ^{13}C NMR spectrum of (*R*)-IPO-glucuronide

Supplemental Figure 4: HSQC NMR spectrum of (*R*)-IPO-glucuronide

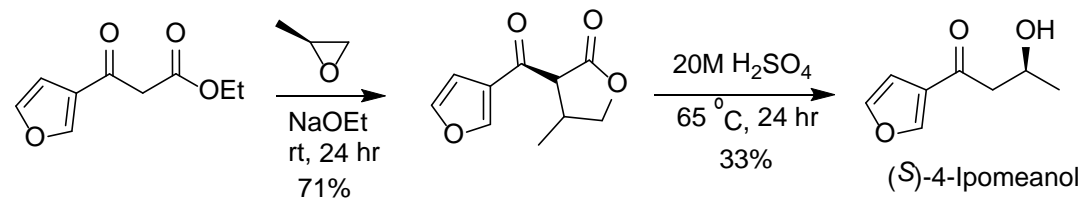
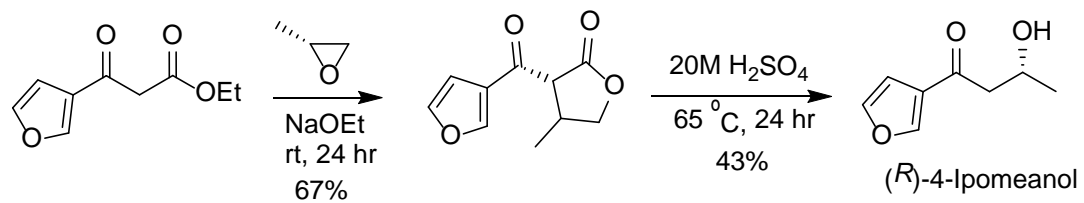
Supplemental Figure 5: HRMS of (*R*)-IPO-glucuronide

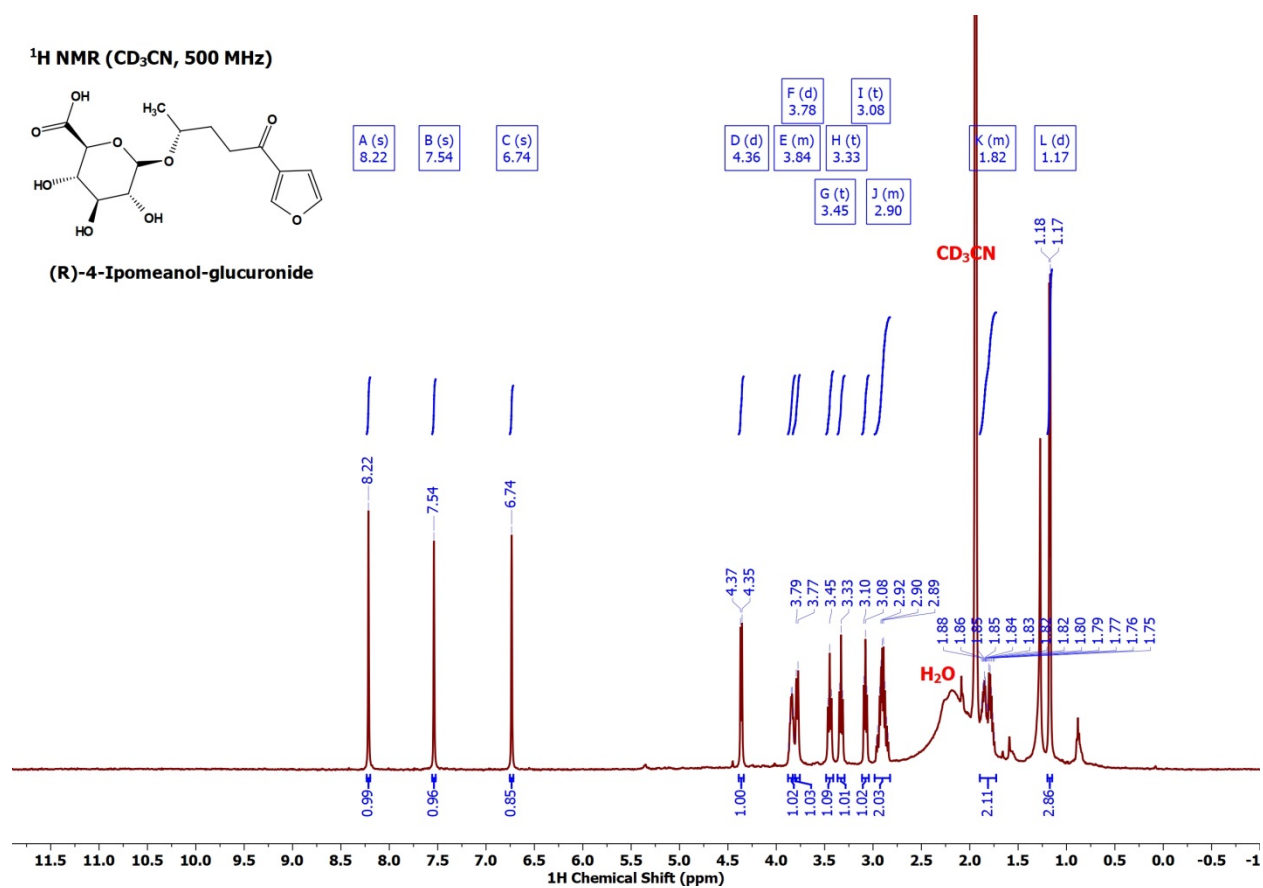
Supplemental Figure 6: ^1H NMR spectrum of (*S*)-IPO-glucuronide

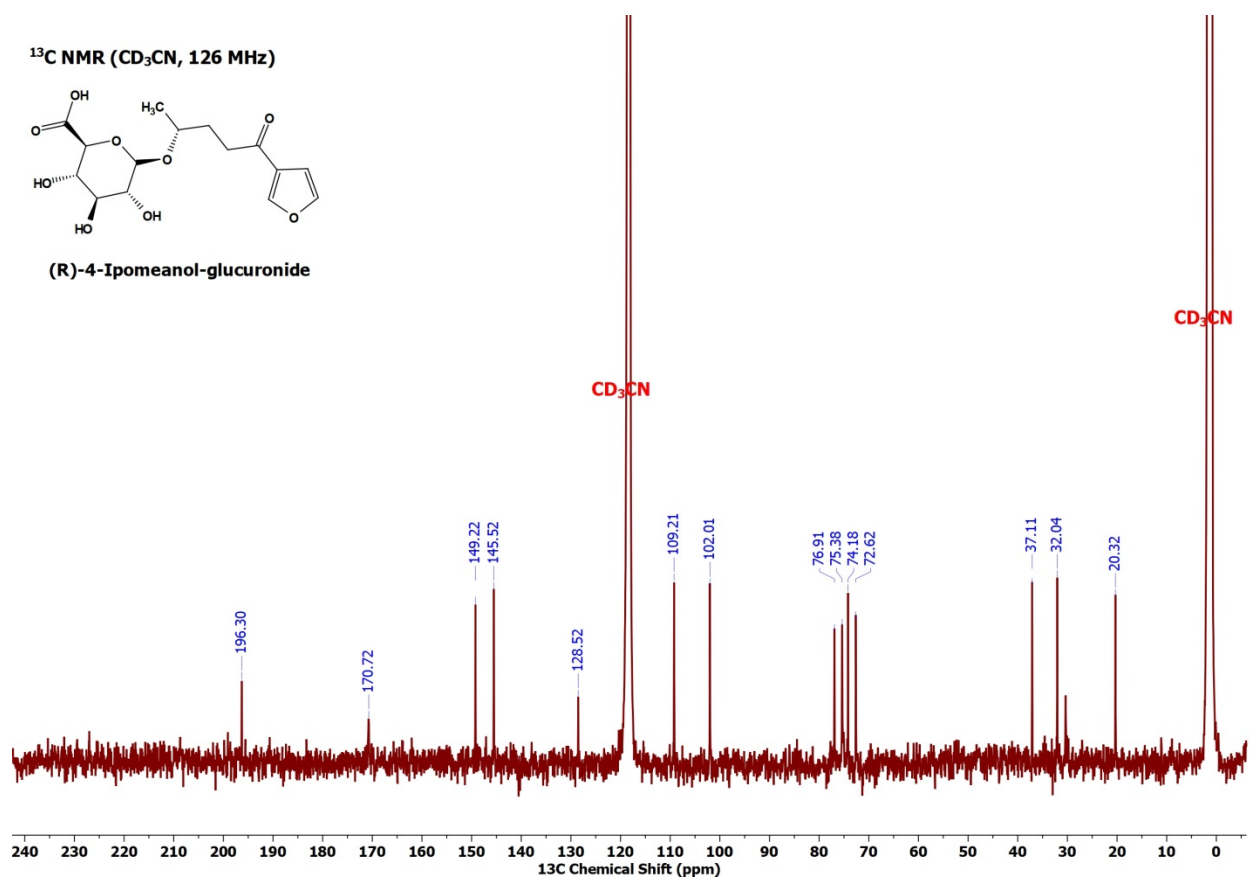
Supplemental Figure 7: ^{13}C NMR spectrum of (*S*)-IPO-glucuronide

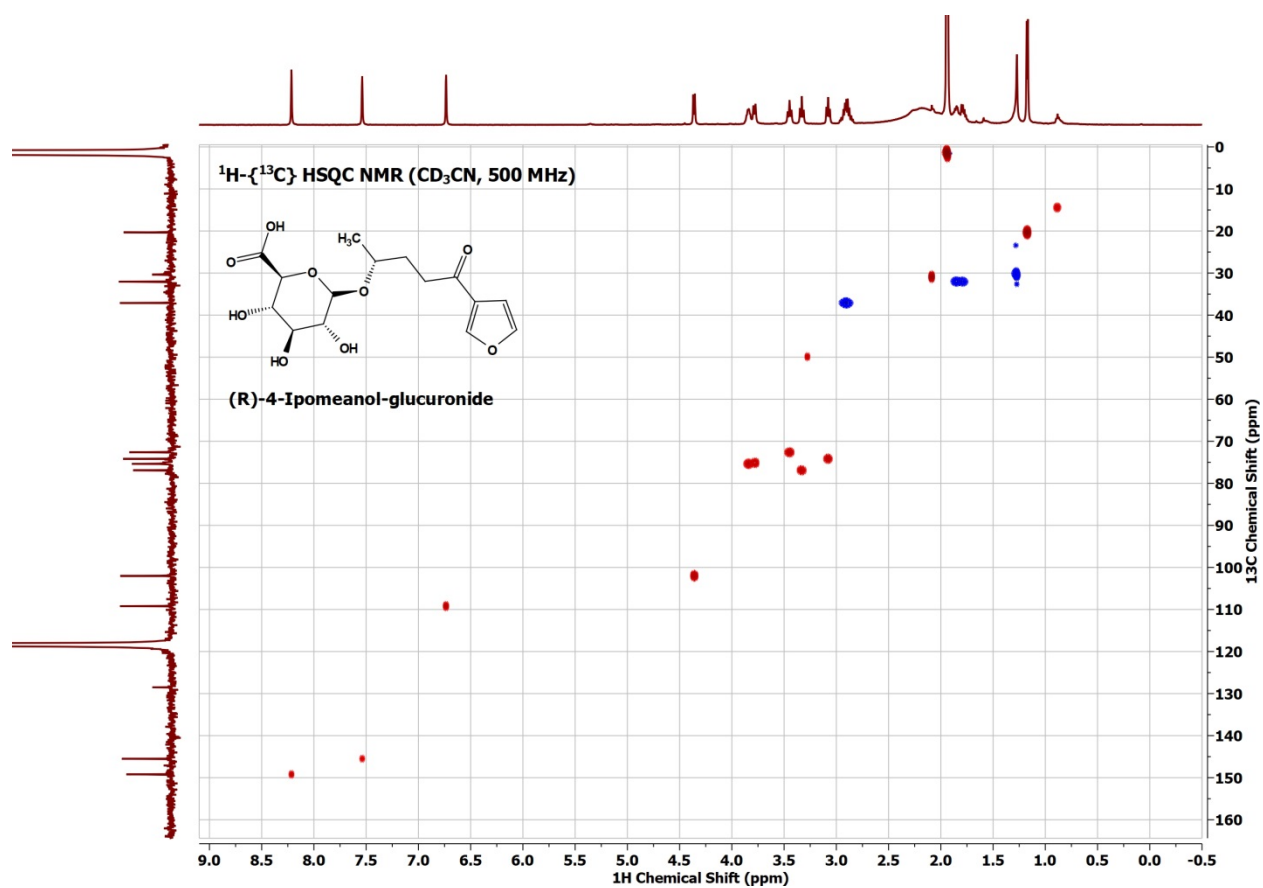
Supplemental Figure 8: HSQC NMR spectrum of (*S*)-IPO-glucuronide

Supplemental Figure 9: HRMS of (*S*)-IPO-glucuronide

Supplemental Figure 1: Synthetic Scheme for of (*R*)- and (*S*)-4-Ipomeanol

Supplemental Figure 2: ¹H NMR spectrum of (*R*)-IPO-glucuronide

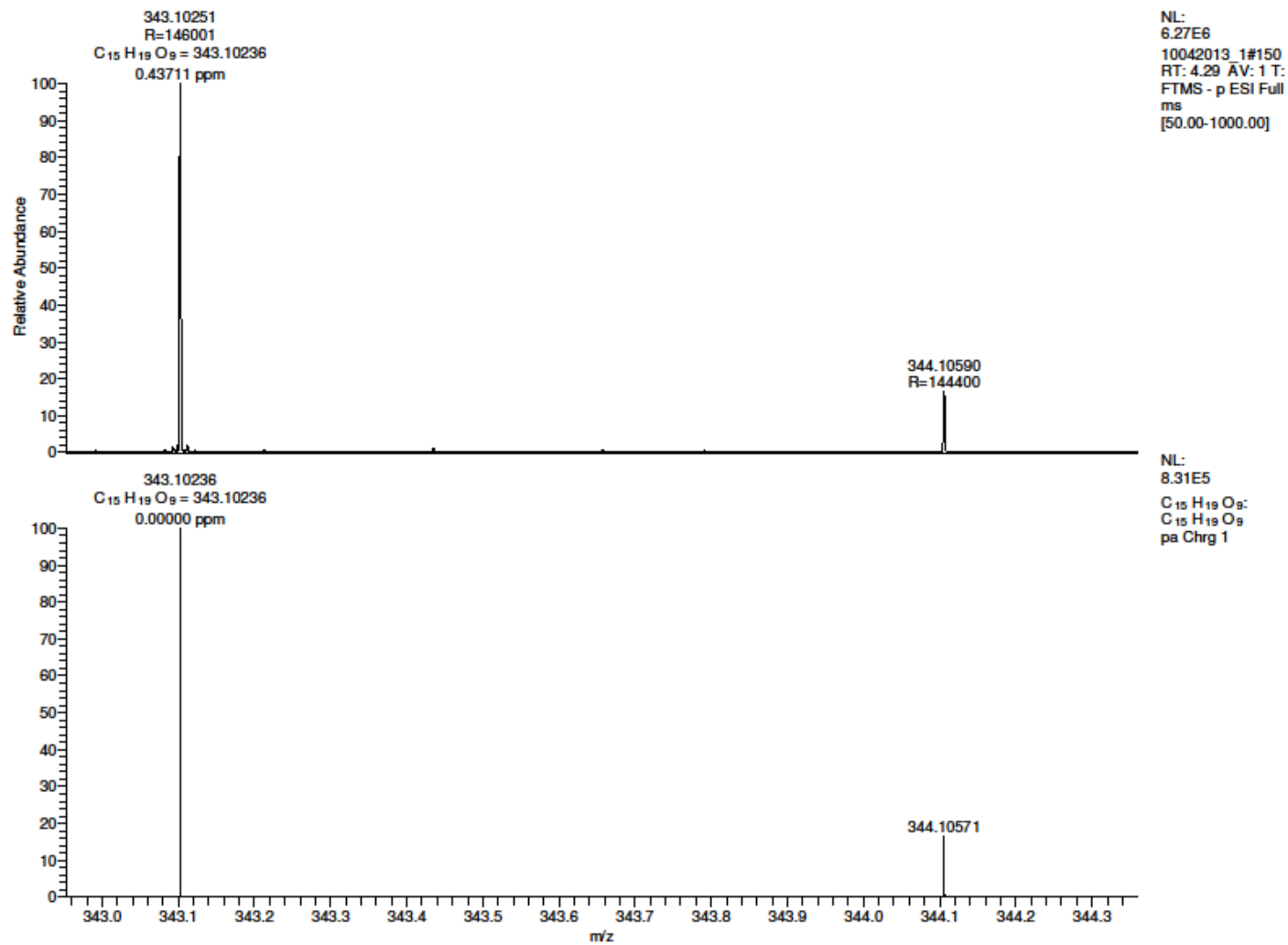
Supplemental Figure 3: ^{13}C NMR spectrum of (*R*)-IPO-glucuronide

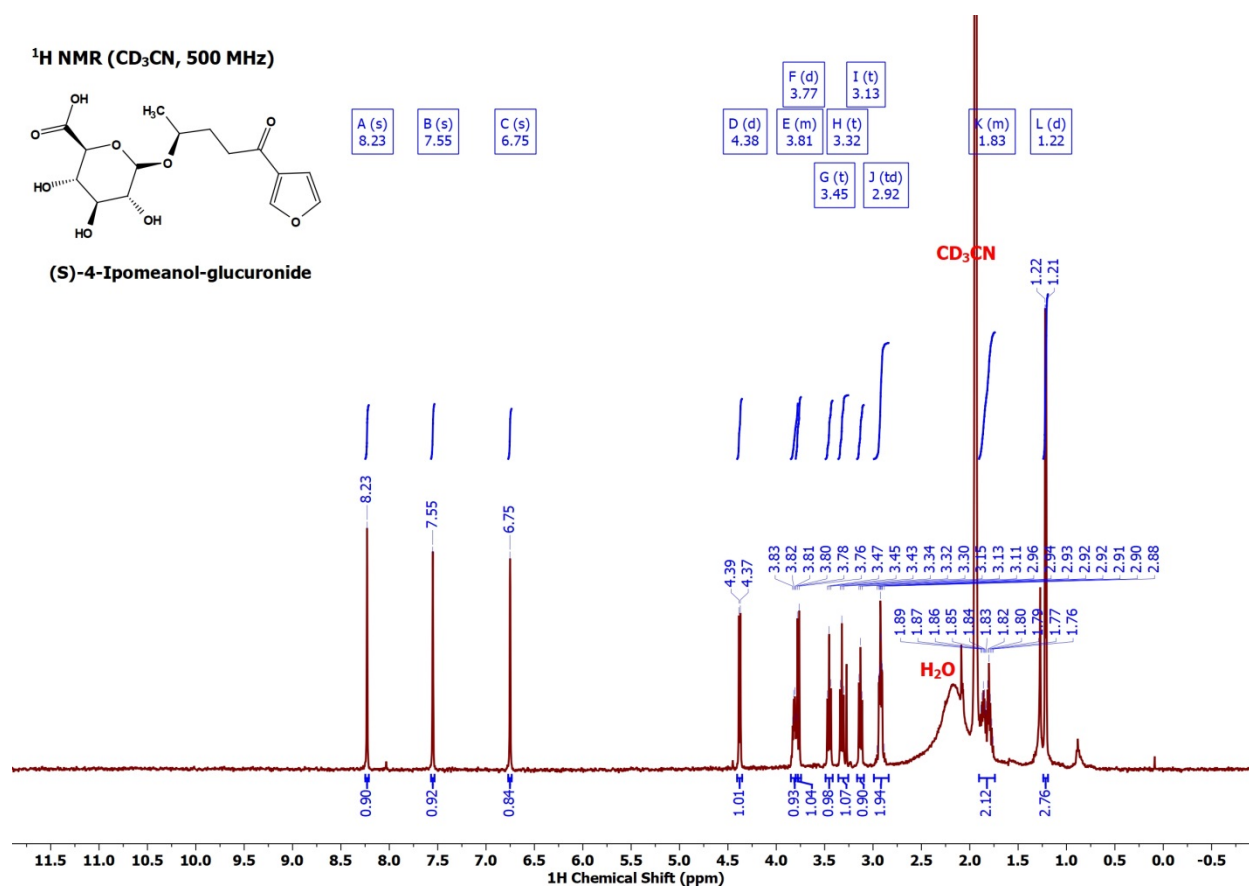
Supplemental Figure 4: HSQC NMR spectrum of (*R*)-IPO-glucuronide

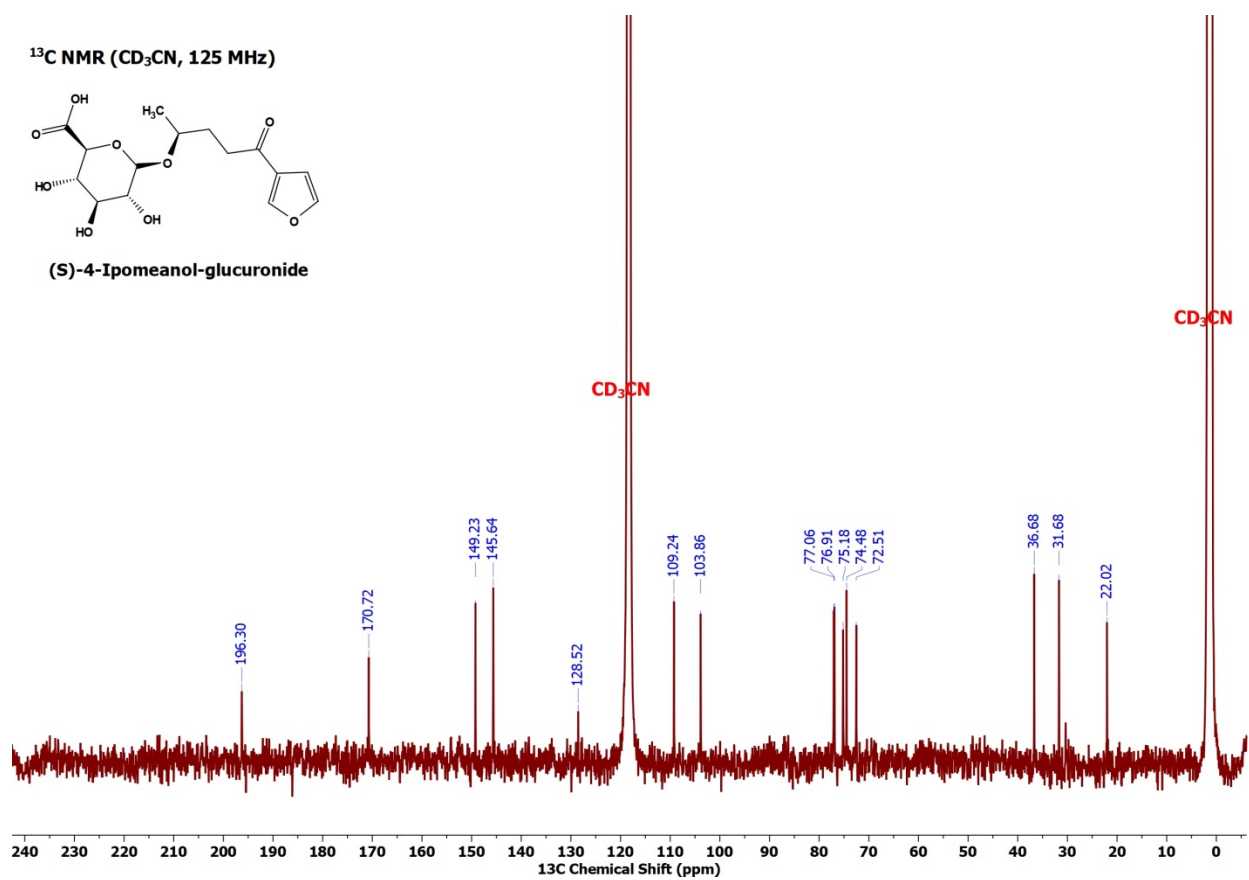
Supplemental Figure 5: HRMS of (*R*)-IPO-glucuronideD:\Xcalibur\...Aaron\10042013_1
4-Ipo-Gluc

10/4/2013 10:45:45 AM

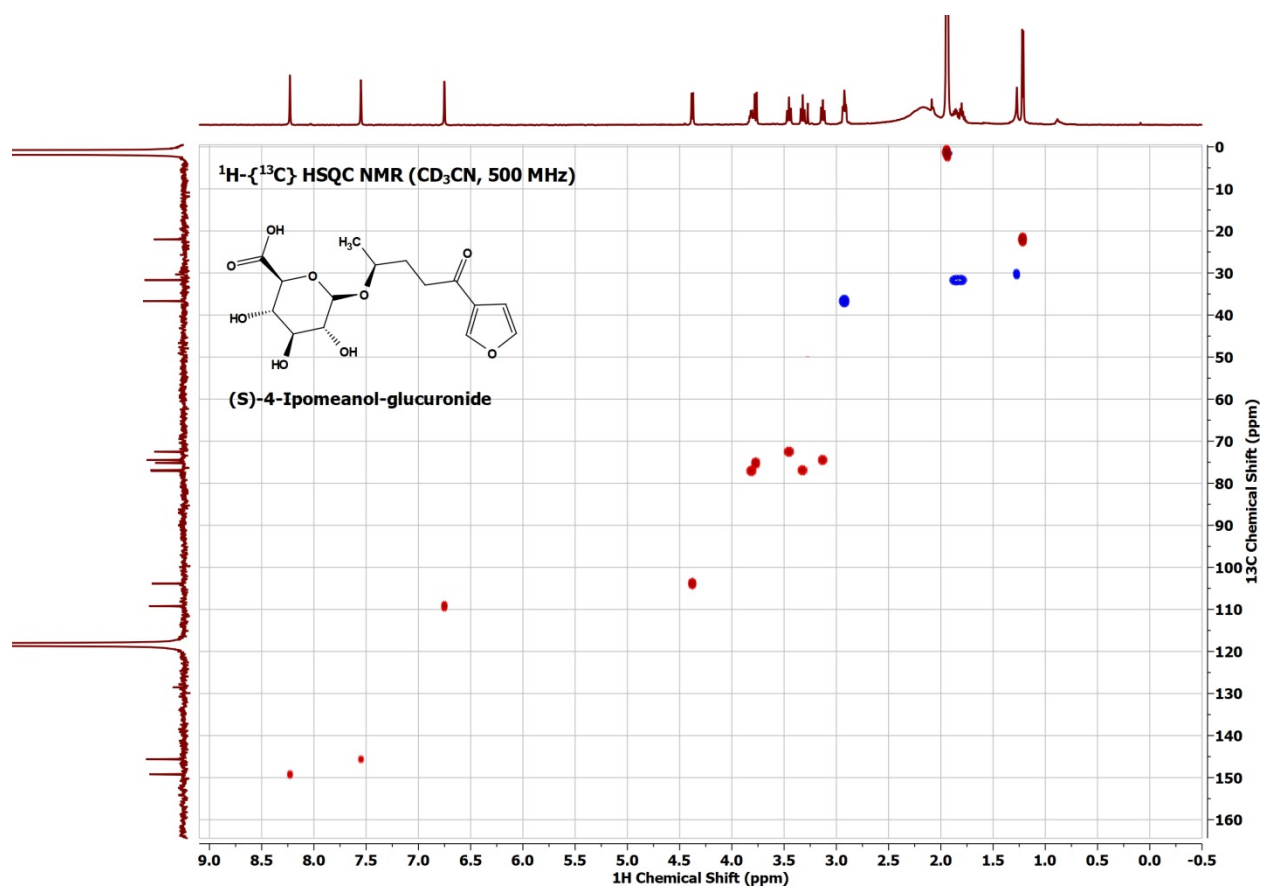
res 100K; new calibration



Supplemental Figure 6: ¹H NMR spectrum of (S)-IPO-glucuronide

Supplemental Figure 7: ^{13}C NMR spectrum of (S)-IPO-glucuronide

Supplemental Figure 8: HSQC NMR spectrum of (S)-IPO-glucuronide



Supplemental Figure 9: HRMS of (S)-IPO-glucuronide

D:\Xcalibur\...Aaron\10042013_1
4-Ipo-Gluc

10/4/2013 10:45:45 AM

res 100K; new calibration

